Composites Science and Technology 72 (2012) 152–158

Contents lists available at SciVerse ScienceDirect

Composites Science and Technology

journal homepage: www.elsevier.com/locate/compscitech

Evolution of interfacial nanostructures and stress states in Mg matrix composites reinforced with coated continuous carbon fibers

W.G. Wang, B.L. Xiao, Z.Y. Ma *

Shenyang National Laboratory for Materials Science, Institute of Metal Research, Chinese Academy of Sciences, 72 Wenhua Road, Shenyang 110016, China

ARTICLE INFO

Article history:
Received 26 July 2011
Received in revised form 15 October 2011
Accepted 19 October 2011
Available online 25 October 2011

Keywords:
A. Metal–matrix composites (MMCs)
A. Carbon fibers
E. Sol–gel methods
B. Interface
C. Stress relaxation

ABSTRACT

Magnesium (Mg) matrix composites reinforced with 45 vol.% continuous carbon fibers (C_f) were fabricated using a pressureless infiltration process in vacuum. In order to modify the interface between the C_f and the Mg matrix, the C_f were coated with 5.0 mol.% yttria stabilized zirconia (YSZ) in sol–gel route. The C_f/Mg composite exhibited a tensile strength of 1.08 GPa which reached 90% of the theoretical prediction by means of the rule of mixture. Microstructural examinations revealed the occurrence of interfacial reaction between the YSZ coating and the Mg matrix, producing a ~20 nm thick interfacial reaction layer consisting of nanocrystalline particles, which include MgO particles, remaining ZrO_2 particles and a small quantity of ZrC particles. Interfacial reaction could induce a large compressive stress in the interfacial layer. As a result, some nanostructured defects, such as edge dislocations, were formed in interfacial layer due to the compressive stress. In the cooling process of fabricating the composite, the phase transformation of the remaining ZrO_2 from tetragonal to monoclinic could relax the thermal residual stress of interfacial layer.

1. Introduction

Carbon fiber (C_f) reinforced metal matrix composites (CfMMCs) are desirable due to their high specific strength and specific modulus, low coefficient of thermal expansion (CTE), etc., compared with conventional alloys. They have been identified as potential candidate materials for primary structural applications not only in the aircraft and aerospace industries but also in the automobile industry and other fields [1–5].

Various processing routes for the CfMMCs have been developed, and liquid metal infiltration under an external force has emerged as the most common fabrication method [5–7]. Since the wetting between carbon fiber and liquid metal is poor and carbon can react with many metal elements in the processes of fabricating the CfMMCs, interfacial wetting and reaction controlling are very important for enhancing the properties of the CfMMCs [5,6,8–10].

Using sol–gel coating to modify the C_f surfaces is a very efficient method of overcoming these obstacles in the fabrication process of the CfMMCs [9,10]. Chen and Li [9] prepared the SiO_2 coating on the C_f with the sol–gel method and fabricated the C_f/Mg composite using a pressure infiltration process in vacuum. It was revealed that the interfacial reaction product was MgO. The tensile strength of 32 vol.% and 40 vol.% C_f reinforced ZM5 Mg alloy was 489 MPa and 663 MPa, respectively. Wu et al. [11] fabricated a 55 vol.% C_f reinforced AZ81 Mg matrix composite by a pressure infiltration casting method, with a ~50 nm thick SiC amorphous coating. The biggest tensile strength was 1038 MPa, about 70% of the theoretical value. Additionally, it was reported that Al_2O_3 coatings could prevent the interfacial reaction between C_f and Al and improve the tensile strength of the C_f/Al composites [10].

Nevertheless, it should be pointed out that the reported tensile strengths of the CfMMCs are significantly lower than those predicted by the rule of mixture, though the surface coating of C_f could enhance the mechanical properties of the CfMMCs to a certain extent. The mechanical properties of the CfMMCs can still be considerably improved. Since the interface plays an important role in determining the physical and mechanical properties of the metal matrix composites (MMCs) [6–10,12–15] and many sol–gel coatings of C_f are nanostructured [16,17], it is necessary to study the interfacial nanostructures for the purposes of optimizing the interfaces and improving the mechanical properties of CfMMCs.

Moreover, the residual stress is a crucial parameter influencing the performances of interfacial layers [18–20]. The study of Huang et al. indicated that the thermal residual stress (TRS) of the TiB_2 interfacial layer on SiC fibers could reach 1.6 GPa [20]. It should be pointed out that the CTE of C_f is greatly lower than that of SiC fibers. This means that the effects of interfacial TRS on the CfMMCs are more significant. Unfortunately, to our knowledge no study has been reported concerning the relaxation of TRS of interfacial layer.

It was reported that the ZrO_2 phase transformation from tetragonal to monoclinic reduced the tensile TRS so much that it changed

* Corresponding author. Tel./fax: +86 24 83978908.
E-mail address: zyma@imr.ac.cn (Z.Y. Ma).

0266-3538/$ - see front matter © 2011 Elsevier Ltd. All rights reserved.
doi:10.1016/j.compscitech.2011.10.008

into compressive stress in a $MoSi_2/ZrO_2$ composite due to volume expansion [21]. Moreover, transformation toughening using ZrO_2 was widely reported in many ceramics [22–24]. In this study, the surfaces of continuous carbon fibers were modified by 5.0 mol.% yttria stabilized zirconia (YSZ) coatings in sol–gel route and the C_f/Mg composites were fabricated using a pressureless infiltration process in vacuum. Special attentions were focused on the evolution of interfacial nanostructures and stress status. Finally, the interrelationship among interfacial reaction, interfacial nanostructures (including phase transformation in interfacial layer), stress statues and tensile properties of CfMMCs were discussed.

2. Experimental procedures

2.1. Preparation of C_f preforms

Unidirectionally aligned high strength carbon fibers (made in China) were used in this study. The preforms of $60 \times 25 \times 5$ mm^3 containing about 45 vol.% C_f were prepared by a filament winding technique. In order to remove the sizing agent on the surfaces of C_f, the preforms were heated at 450 °C for 30 min in a vacuum furnace. After removing the sizing agent, the tensile strength of C_f was 2.6 GPa, according to the ASTM D3379-75 standard.

2.2. Preparation of YSZ sol and coating procedures

YSZ sol was prepared using zirconium oxychloride octahydrate ($ZrOCl_2{\cdot}8H_2O$) and yttrium nitrate hexahydrate ($Y(NO_3)_3{\cdot}6H_2O$) as the precursors. The $ZrOCl_2{\cdot}8H_2O$ and $Y(NO_3)_3{\cdot}6H_2O$ were dissolved in deionized water with a mole ratio of 19:1. Then, anion exchange resin was added to the precursor solution slowly under vigorous stirring until the PH value reached 3.1, and a transparent YSZ sol with a mole concentration of 0.2 mol/l was obtained. The rate of addition of the anion exchange resin should be kept very slow in order to avoid the precipitation of hydroxides. The used anion exchange resin could be recycled, after it is washed with sodium hydroxide solution and deionized water, respectively.

The C_f preforms were immerged in the obtained YSZ sol and ultrasonically vibrated for 10 min, and then removed from the YSZ sol and dried in the shade.

2.3. Fabrication of C_f/Mg composite

A commercial pure Mg matrix composite reinforced with 45 vol.% C_f was fabricated using a pressureless infiltration process in vacuum. At first, Mg ingots and C_f preforms were sealed in a steel die and heated in a vacuum furnace to 635 °C, and the temperature was maintained for 30 min (platform I) for the sake of the calcinations of the YSZ coating (Fig. 1). Liquid metal infiltration was carried out at 750 °C for 20 min (platform II) to form the C_f/Mg composite samples. After the infiltration, two cooling routes were used to study the effects of interfacial nanostructures on the mechanical properties of C_f/Mg composites. For sample A, the infiltrated sample was cooled down directly in the vacuum furnace, whereas for sample B, following the infiltration, the sample was cooled to 650 °C, kept at 650 °C for 60 min (platform III), and then cooled down (Fig. 1). The additional heat-treatment at 650 °C for 60 min aimed to promote the interfacial reaction and eliminate the ZrO_2 in the interfacial layer.

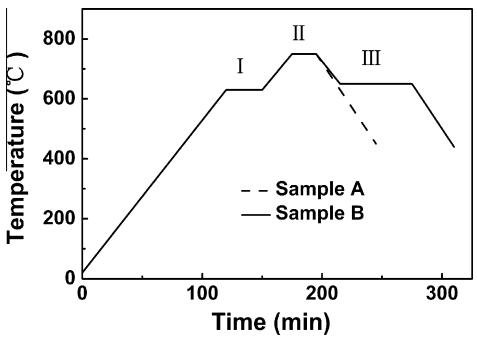

Fig. 1. The temperature curves of fabricating samples A and B.

2.4. Characterization

The microstructures of the YSZ coating and the C_f/Mg composite were examined using scanning electron microscopy (SEM, Nova NanoSEM 430) and transmission electron microscopy (TEM, F20). Thin foils for TEM were prepared by the ion milling technique.

In order to study solely the thermal stability of the YSZ coating (excluding the effects of TRS), the YSZ was coated on alumina substrate that has a similar CTE to the YSZ coating. Consistent with the fabrication parameters of the C_f/Mg composites, one specimen of the YSZ coatings was calcinated at 635 °C for 30 min, while the other was sintered at 635 °C and 750 °C for 30 min at each temperature. These specimens were analyzed using the X-ray diffraction (XRD) technique on a D/max 2500PC diffractometer using Cu Kα radiation.

Tensile tests were conducted at room temperature and an initial strain rate of 3.3×10^{-4} s^{-1}.

3. Results

3.1. The characteristics of YSZ coatings

Fig. 2a shows the coarse surfaces of unsized C_f. After calcination at 635 °C for 30 min, a uniform and smooth YSZ film could be coated on the surfaces of C_f, as shown in Fig. 2b. In addition, no crinkle and crack were found on the YSZ film. These indicate that an excellent YSZ coating was formed on the C_f surfaces.

Fig. 3 shows the XRD patterns taken from the YSZ films coated on the alumina substrates. The YSZ coating consisted of tetragonal ZrO_2 after calcination at 635 °C for 30 min, and no characteristic peak of monoclinic ZrO_2 was found. Similarly, for the coating sintered at 635 °C and 750 °C for 30 min each, only tetragonal ZrO_2 was detected. This indicates that YSZ coating had good thermal stability even in the process of fabricating the C_f/Mg composites from 750 °C to room temperature.

3.2. The microstructures and tensile properties of C_f/Mg composites

Fig. 4a and b shows the cross-sectional SEM micrographs of samples A and B, respectively. The molten Mg infiltrated completely the interspaces among the C_f without additional infiltrating force. It indicates that the YSZ coating could improve the wetting between the C_f and the Mg matrix greatly. The interfacial bonding between the C_f and the Mg matrix was very good without discernible debonding or micro-crack. No obvious difference could be found between samples A and B under SEM.

Fig. 5 shows the TEM microstructures of the interfaces in samples A and B. It can be seen that the surfaces of the C_f were wrapped with a thin and uniform interfacial layer. Selected area diffraction patterns (SADP) shown at the top right corner of Fig. 5a were taken from the interfacial layer and the Mg matrix in sample A. The discontinuous circular SADP indicated that the interfacial layer consisted of some tiny particles with sizes on the order of nanometers. Under a submicron scale, it was difficult to

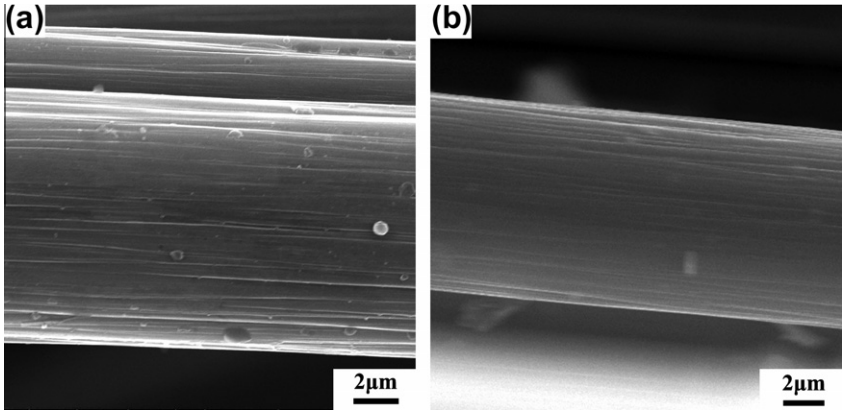

Fig. 2. SEM images of (a) unsized C_f and (b) C_f coated with YSZ sol after calcination at 635 °C for 30 min.

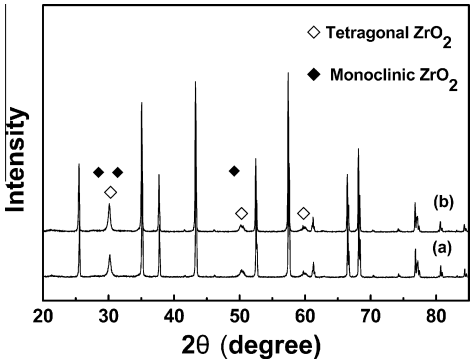

Fig. 3. XRD patterns of YSZ films coated on alumina substrates sintered (a) at 650 °C for 30 min and (b) at 650 °C and 750 °C, respectively, for 30 min.

find any difference between the interfacial layers of samples A and B.

The tensile strengths of samples A and B were 1.08 GPa and 0.93 GPa, respectively. The tensile strength of sample A reached 90% of the theoretical value predicted by the rule of mixture. This indicates that the interface bonding between the C_f and the Mg matrix in sample A was very good and that the C_f did not suffer from significant damage during the composite fabrication process. The tensile strength of sample B was lower than that of sample A.

3.3. The nanostructures of interfacial layers

Fig. 6a shows the HRTEM image of the interfacial layer in sample A, and at least four particles could be conspicuously observed. They were determined to be MgO particles and ZrO_2 particles, respectively. MgO was the primary component of the interfacial layer, and no orientation relationship was found among the MgO particles. In order to reveal the nanostructure clearly, a magnified view of the grain boundary between MgO particles is shown in Fig. 6b. A disordered intergranular film could be observed between MgO particles. The HRTEM examinations indicated that the Mg matrix reacted with the YSZ coating to form the MgO as follows:

$$ZrO_2 + 2Mg \rightarrow 2MgO + Zr \quad (1)$$

As shown in Fig. 6a, the ZrO_2 particle remained at the surface of the C_f and was covered completely by the MgO particles. It is thought that the MgO particle layer was a good barrier for restraining interfacial reaction between the Mg matrix and the remaining ZrO_2 particles. Moreover, it was confirmed that the crystalline phase of the remaining ZrO_2 particle was monoclinic. According to the foregoing XRD analysis (Fig. 3), the tetragonal ZrO_2 could be obtained after calcinations at 635 °C for 30 min and exhibited very good thermal stability at 750 °C. Obviously, some other factors play a role and they drove the ZrO_2 particles from tetragonal phase to monoclinic phase during the fabrication process of the C_f/Mg composite.

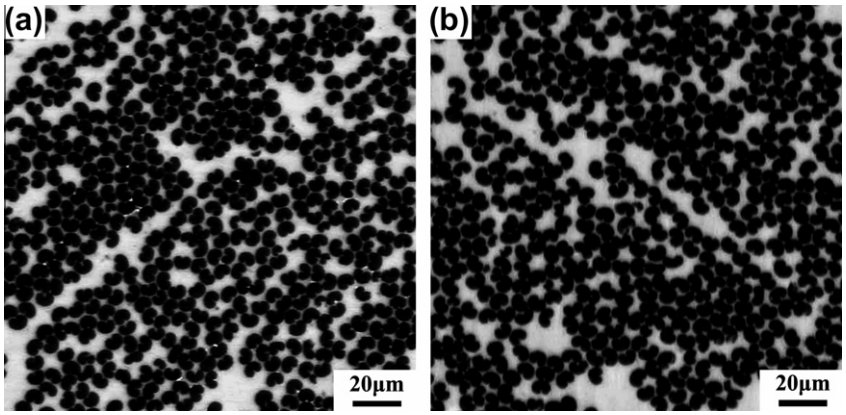

Fig. 4. SEM micrographs showing microstructures of (a) sample A and (b) sample B.

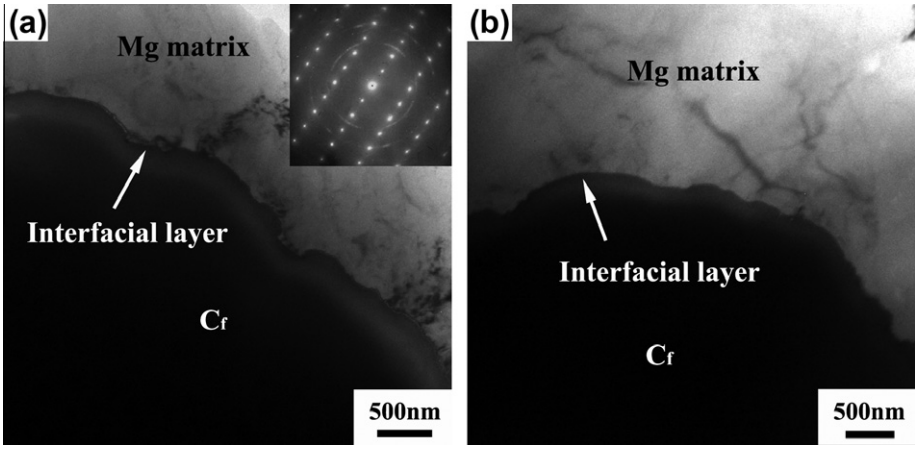

Fig. 5. TEM images showing interfacial microstructure of (a) sample A and (b) sample B.

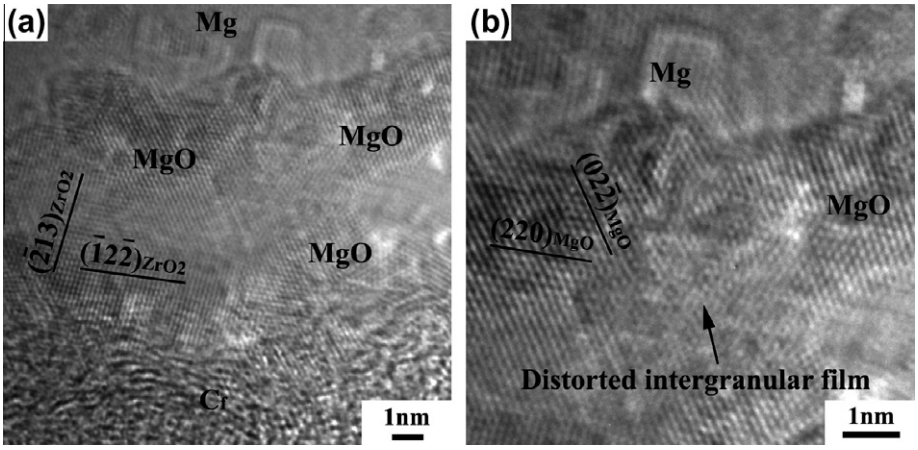

Fig. 6. HRTEM images showing (a) interfacial nanostructures of sample A and (b) locally magnified image of figure (a).

Fig. 7a shows the HRTEM image of the interfacial layer in sample A. A ZrC particle was found on the surface of C_f with a size of about 3 nm. This indicates that Zr diffused to the surface of C_f and reacted with C_f to form ZrC as follows:

$$Zr + C \rightarrow ZrC \quad (2)$$

In sample A, the quantity of ZrC particle was very small. It is thought that the majority of the deoxidized Zr dissolved into the molten Mg matrix during the fabrication of the C_f/Mg composite. Moreover, Inverse Fast Fourier Transform (IFFT) is carried out to analyze the nanostructure with Digital Micrograph. Fig. 7b and c are the IFFT images taken from regions B and C which are framed with white lines in Fig. 7a, corresponding to the MgO particle and ZrC particle, respectively. It is important to note that dislocations were found in both the MgO and the ZrC particles as marked by black lines in Fig. 7b and c. Nevertheless, no dislocation was found in the remaining ZrO_2 particles with a monoclinic structure.

Fig. 8a shows the interfacial nanostructures in sample B. No remaining ZrO_2 particle was found and the interfacial layer consisted mainly of MgO particles. Fig. 8b is the IFFT image taken from the region framed with the white lines in Fig. 8a. With the progress of the interfacial reaction, some lattices of the MgO particles were distorted, and the lattice damage degree in sample B was severer than that in sample A. It is thought that the lattice damage of interfacial layer is a crucial parameter determining the performances of interfacial layers and mechanical properties of CfMMCs.

4. Discussion

For sample A, a tensile strength of 1.08 GPa, which reached 90% of the theoretical prediction, was obtained. Such a high strength is attributed to excellent interfacial nanostructure. Moreover, the TRS is an important factor that must be taken into consideration. In order to provide scientific basis for the interface optimization, the internal relationships among interfacial reaction, interfacial nanostructures (including phase transformation in interfacial layer), interfacial stress states and mechanical properties of CfMMCs should be studied in depth.

4.1. The effects of interfacial reaction on interfacial nanostructures

After calcinations at 635 °C for 30 min, a smooth YSZ coating was obtained on the surfaces of C_f, and the crystalline phase of ZrO_2 was tetragonal. In the processes of fabricating the composites, Mg reacted with ZrO_2 particles in the YSZ coatings to form MgO nanocrystalline particles. As the deoxidization product, most of the Zr was dissolved into the molten Mg matrix, and a small quantity of Zr diffused to the surfaces of C_f and reacted with C_f to form ZrC nanocrystalline particles about 3 nm in size on the surfaces of C_f, as shown in Fig. 7. As the products of interfacial reaction, the MgO particles acted as a good barrier in restraining the interfacial reaction. As a result, a small quantity of ZrO_2 particles remained on the C_f surfaces and was covered by the MgO particles completely.

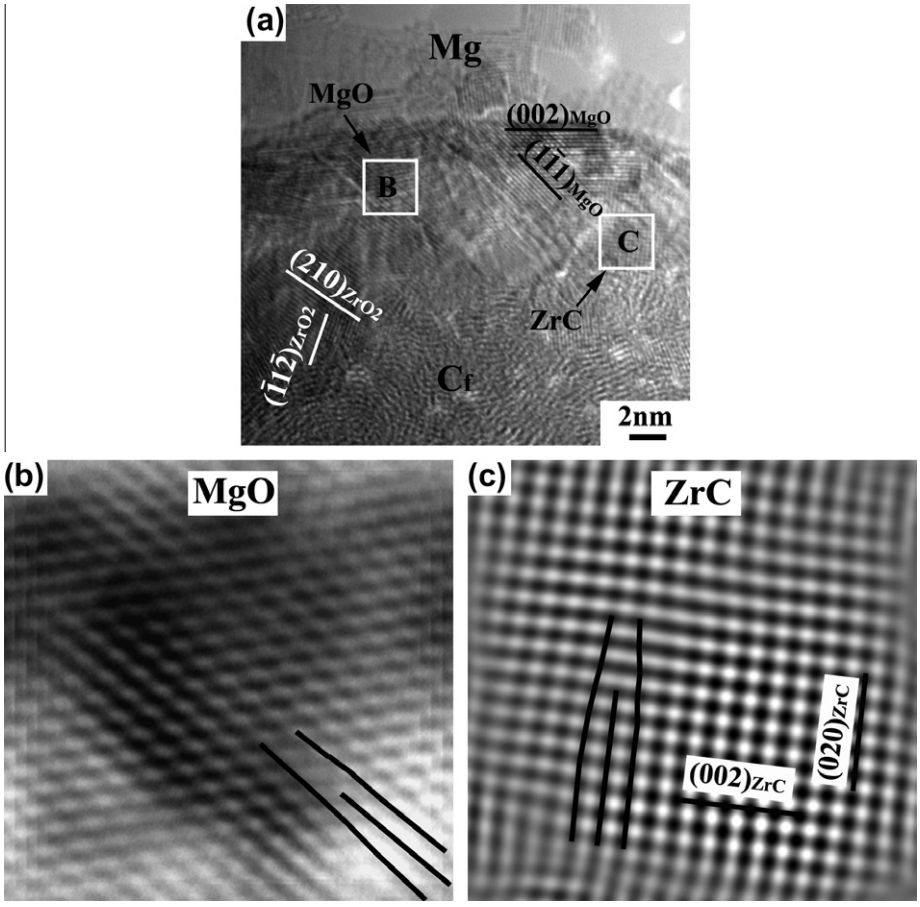

Fig. 7. (a) HRTEM image of interfacial layer in sample A, (b) and (c) IFFT of regions B and C framed with white squares in figure (a).

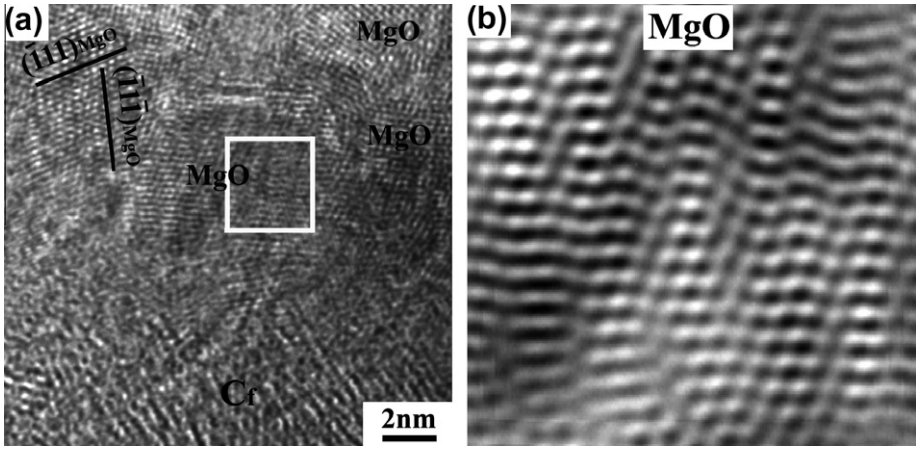

Fig. 8. (a) HRTEM image of interfacial layer in sample B with an additional heat-treatment (at 650 °C for 60 min) after liquid metal infiltration and (b) IFFT of region framed with white square in figure (a).

It was reported that the YSZ coating consisted of nanostructured particles after calcinations [16], and some pores several nanometers in size could be formed in the calcination process [17]. In this study, no pore was observed in the interfacial layers (Figs. 6 and 7). Taking into account the formation of the ZrC particles, it is believed that the ZrC particles filled up the space of pores in the YSZ coating. In the CfMMCs such as the Al-based CfMMCs, the purpose of modifying the C_f surfaces is not only improving the wetting and interfacial bonding strength but also controlling the interfacial reaction. Obviously, the existence of pores in the YSZ coating was unbeneficial to the purposes of the surface modification of C_f. Therefore, it is thought that the formation of the ZrC particles was beneficial to the densification of the interfacial layer, restraining the interfacial reaction and improving the interfacial mechanical properties.

4.2. The effects of interfacial reaction on stress states

According to Eq. (1), 1 mol of ZrO_2 would form 2 mol of MgO, and the volumes of ZrO_2 and MgO is 20.74 cm^3 and 22.35 cm^3,

respectively. Since the majority of the deoxidized Zr dissolved into the molten Mg matrix, the volume change caused by the interfacial reaction could be calculated as follows:

$$(22.35\ \mathrm{cm}^3 - 20.74\ \mathrm{cm}^3)/20.74\ \mathrm{cm}^3 \approx 7.8\% \quad (3)$$

It is obvious that the interfacial reaction would bring on a volume expansion. Further, a compressive stress field could be formed in the interfacial layer. And the volume expansion rate of interfacial layer exceeds greatly the range of elastic deformation of brittle ceramics.

4.3. The effects of stress states on interfacial nanostructures

As shown in Fig. 7, the edge dislocations were found in both MgO and ZrC particles in the interfacial layer, and disordered intergranular films could be observed between MgO particles. This seems surprising, considering that both MgO and ZrC are brittle ceramic particles. According to previous studies, nanocrystalline ceramics have an increased volume fraction of disordered intergranular films, which were observed both experimentally [25,26] and by means of molecular dynamics simulations [27]. Multimillion-atom molecular dynamics simulations of nanocrystalline SiC [28] revealed unusual deformation mechanisms, resulting from the coexistence of brittle grains and soft amorphous grain boundary phases. Simulations predicted a crossover from an intergranular continuous deformation to an intragrain discrete deformation at a critical indentation depth under indenter load [28]. Moreover, Bobylev et al. [29] calculated the critical stress needed for athermal formation of dislocations in nanocrystalline SiC.

In this study, the nanocrystalline particles and disordered intergranular boundaries in the interfacial layer were found, as shown in Fig. 6b. Moreover, the edge dislocations were observed in the nanocrystalline MgO and ZrC particles (Fig. 7). The formation of these edge dislocations in the MgO and ZrC particles should be attributed to the unusual deformation mechanisms of nanocrystalline ceramics and a large compressive stress.

According to the previous analysis, a large compressive stress could be induced due to the volume expansion caused by the interfacial reaction. With the progressing of the interfacial reaction, the compressive stress increased. When the compressive stress was large enough to exceed the critical stress needed for the formation of dislocations in the nanocrystalline particles, the edge dislocations were formed in both the MgO and the ZrC particles. This viewpoint is further confirmed by the interfacial nanostructures in sample B. When all the ZrO_2 reacted with the Mg matrix, the lattice defects in sample B became severer than those in sample A, and the thickness of soft amorphous grain boundary phases was wider than that in sample A, as shown in Figs. 6 and 8.

As shown in Fig. 3, the crystalline phase of ZrO_2 should be tetragonal after calcinations at 635 °C for 30 min. However, HRTEM observations showed that all the remaining ZrO_2 particles in the interfacial layer were monoclinic, indicating the occurrence of the phase transformation of ZrO_2 from tetragonal to monoclinic. This phase transformation would induce a volume expansion [26,30]. It was reported that the compressive stress would restrain the occurrence of the phase transformation of ZrO_2 from tetragonal to monoclinic [30]. Taking into account the good thermal stability of tetragonal ZrO_2 particles at 750 °C and the inhibition of compressive stress to the phase transformation, it is impossible for the phase transformation of all ZrO_2 particles to occur during liquid metal infiltration or in large compressive stress states.

Previous studies [31,32] documented that the stress state was an important factor which could change the thermal stability of tetragonal ZrO_2. Benali et al. [31] and Qin et al. [32] suggested that tensile stress was beneficial to the phase transformation of ZrO_2 from tetragonal to monoclinic, since this transformation was accompanied by a volume expansion. In addition, Huang et al. [19,20] calculated the TRS of the interfacial layer in a SiC_f/Ti–6Al–4V composite. The maximum of the TRS in the TiB_2 interfacial layer was hoop stress and tensile, and the value of hoop TRS could reach 1.6 GPa. In this study, the mismatch of CTE between the C_f and the MgO interfacial layer was very large. Therefore, it is believed that a large tensile TRS was formed in the interfacial layer of the C_f/Mg composite. Under the tensile TRS, the remaining ZrO_2 transformed from tetragonal phase to monoclinic phase in the cooling process of fabricating the C_f/Mg composite.

Moreover, it should be noted that no dislocation was found in the remaining ZrO_2 particles, though the elastic modulus of the tetragonal ZrO_2 is similar to that of MgO and lower than that of ZrC. It is suggested that the dislocations might be formed originally in the tetragonal ZrO_2 particles and then disappeared due to the rearrangement of lattice during the phase transformation of ZrO_2 from tetragonal to monoclinic.

In summary, the tensile TRS triggered the ZrO_2 phase transformation, and the phase transformation reduced the nanostructured defects such as dislocations in the interfacial layer of the C_f/Mg composite.

4.4. The effects of nanostructures on stress states

It was documented that the ZrO_2 phase transformation from tetragonal to monoclinic could decrease the tensile TRS so much that it would change into compressive stress in $MoSi_2/ZrO_2$ composite due to the volume expansion [21]. In this study, the tensile TRS of the interfacial layer could be relaxed to some extent because of the phase transformation of the remaining ZrO_2.

In summary, two points should be considered when optimizing the interfacial designs for the CfMMCs. First, the volume change caused by the interfacial reaction between coatings and metal matrix will result in the formation of nanostructured defects in the interfacial layer, deteriorating the mechanical properties of the CfMMCs. Second, using phase transformation to relax the large TRS and reduce the nanostructured defects of the interfacial layer is an effective approach to improve the mechanical properties of the CfMMCs.

5. Conclusions

1. Using the sol–gel coating method, a uniform and smooth YSZ coating was obtained on the surfaces of C_f, resulting in greatly improved wetting between C_f and molten Mg. The 45 vol.% C_f/Mg composite was successfully fabricated using the pressureless infiltration process in vacuum, producing a high tensile strength of 1.08 GPa.
2. Mg reacted with the YSZ coating to form the MgO particle interfacial layer with a thickness of about 20 nm. As a product of the interfacial reaction, a small quantity of Zr diffused to the C_f surface and reacted with C_f to form tiny ZrC particles. The MgO interfacial reaction layer was a good barrier in restraining the interfacial reaction. As a result, a small quantity of ZrO_2 particles remained on the C_f surfaces and was covered by the MgO particles. The MgO, ZrO_2 and ZrC particles had sizes of 3–5 nm.
3. A large compressive stress could be formed in the interfacial layer due to the volume expansion caused by the interfacial reaction. As a result, the nanostructured defects, such as edge dislocations, were induced.
4. When the composite was cooled from the infiltration temperature, the stress states of the interfacial layer changed from compressive to tensile. The tensile TRS triggered the

ZrO_2 phase transformation from tetragonal to monoclinic, relaxing the tensile TRS of the interfacial layer and reducing the nanostructured defects of the interfacial layer. Both these two factors were beneficial to the improvement of the tensile strength of the C_f/Mg composite.

Acknowledgements

The authors gratefully acknowledge the support of the National Basic Research Program of China under Grant No. 2006CB605306 and the China Postdoctoral Science Foundation.

References

[1] Miracle DB. Metal matrix composites – from science to technological significance. Compos Sci Technol 2005;65:2526–40.
[2] Hufenbach W, Andrich M, Langkamp A, Czulak A. Fabrication technology and material characterization of carbon fibre reinforced magnesium. J Mater Process Technol 2006;175:218–24.
[3] Rawal S. Metal-matrix composites for space applications. JOM 2001;53(4):14–7.
[4] Evans A, Marchi CS, Mortensen A. Metal matrix composites in industry. Kluwer Academic Publisher; 2003.
[5] Wu F, Zhu J. Morphology of second-phase precipitates in carbon–fiber- and graphite–fiber–reinforced magnesium-based metal-matrix composites. Compos Sci Technol 1997;57:661–7.
[6] Feldhoff A, Pippel E, Woltersdorf J. Interface engineering of carbon–fiber reinforced Mg–Al alloys. Adv Eng Mater 2000;2:471–80.
[7] Shalu T, Abhilash E, Joseph MA. Development and characterization of liquid carbon fibre reinforced aluminium matrix composite. J Mater Process Technol 2009;209:4809–13.
[8] Wang YC, Zhou BL. Behaviour of coatings on reinforcements in some metal matrix composites. Compos Part A 1996;27:1139–45.
[9] Chen R, Li X. A study of silica coatings on the surface of carbon or graphite fiber and the interface in a carbonmagnesium composite. Compos Sci Technol 1993;49:357–62.
[10] Rajan TPD, Pillai RM, Pai BC. Review reinforcement coatings and interfaces in aluminium metal matrix composites. J Mater Sci 1998;33:3491–503.
[11] Wu F, Zhu J, Chen Y, Zhang G. The effects of processing on the microstructures and properties of Gr/Mg composites. Mater Sci Eng A 2000;277:143–7.
[12] Yue HY, Wang LD, Fei WD. Improvement of the tensile strength of $Al_{18}B_4O_{33w}$/Al composite at elevated temperatures by change of interfacial state. Mater Sci Eng A 2008;486:409–12.
[13] Clyne TW, Watson MC. Interfacial mechanics in fibre-reinforced metals. Compos Sci Technol 1991;42:25–55.
[14] Gundel DB, Miracle DB. Transverse tensile behavior of SiC–fiber/Ti–6Al–4V composites-1. Experimental results. Compos Sci Technol 1998;58:1571–81.
[15] Gundel DB, Warrier SG, Miracle DB. The transverse tensile behavior of SiC–fiber/Ti–6Al–4V composites 2. Stress distribution and interface failure.. Compos Sci Technol 1999;59:1087–96.
[16] Okubo T, Nagamoto H. Low-temperature preparation of nanostructured zirconia and YSZ by sol–gel processing. J Mater Sci 1995;30:749–57.
[17] Gopalan R, Chang CH, Lin YS. Thermal stability improvement on pore and phase structure of sol–gel derived zirconia. J Mater Sci 1995;30:3075–81.
[18] Shaw LL, Miracle DB. Effects of an interfacial region on the transverse behavior of metal-matrix composites – a finite element analysis. Acta Mater 1996;44:2043–55.
[19] Huang B, Yang Y, Luo H, Yuan M, Chen Y. Effect of the interfacial reaction layer thickness on the thermal residual stresses in SiCf/Ti–6Al–4V composites. Mater Sci Eng A 2008;489:178–86.
[20] Huang B, Yang Y, Luo H, Yuan M. Effects of the coating system and interfacial region thickness on the thermal residual stresses in SiCf/Ti–6Al–4V composites. Mater Des 2009;30:718–22.
[21] Lu GY, Lederich R, Wold Soboyejo W. Residual stresses and transformation toughening in $MoSi_2$ composites reinforced with partially stabilized zirconia. Mater Sci Eng 1996;A210:25–41.
[22] Sergo V, Lughi V, Pezzotti G, Lucchini E, Meriani S, Muraki N, Katagiri G, Casto SL, Nishida T. The effect of wear on the tetragonal-to-monoclinic transformation and the residual stress distribution in zirconia-toughened alumina cutting tools. Wear 1998;214:264–70.
[23] Basua B, Vleugels J, Biest OVD. Microstructure–toughness–wear relationship of tetragonal zirconia ceramics. J Eur Ceram Soc 2004;24:2031–40.
[24] Zhang B, Boey F. The phases and the toughening mechanisms in (Y)ZrO_2–Al_2O_3–(Ti, W)C ceramics system. Mater Lett 2000;43:197–202.
[25] Chen D, Zhang XF, Ritchie RO. Effects of grain boundary structure on the strength, toughness and cyclic-fatigue properties of a monolithic silicon carbide. J Am Ceram Soc 2000;83:2079–81.
[26] Xu X, Nishimura T, Hirosaki N, Xie RJ, Yamamoto Y, Tanaka H. Superplastic deformation of nano-sized silicon nitride ceramics. Acta Mater 2006;54:255–62.
[27] Keblinski P, Phillpot SR, Wolf D, Gleiter H. Amorphous structure of grain boundaries and grain junctions in nanocrystalline silicon by molecular-dynamics simulation. Acta Mater 1997;45:987–98.
[28] Szlufarska I, Nakano A, Vashishta P. A crossover in the mechanical response of nanocrystalline ceramics. Science 2005;309:911–4.
[29] Bobylev SV, Mukherjee AK, Ovidko IA. Emission of partial dislocations from amorphous intergranular boundaries in deformed nanocrystalline ceramics. Scripta Mater 2009;60:36–9.
[30] Bouvier P, Godlewski J, Lucazeau G. A Raman study of the nanocrystallite size effect on the pressure–temperature phase diagram of zirconia grown by zirconium-based alloys oxidation. J Nucl Mater 2002;300:118–26.
[31] Benali B, Ghysel MH, Gallet I, Huntz AM, Andrieux M. Stress driven phase transformation in ZrO_2 film. Appl Surf Sci 2006;253:1222–6.
[32] Qin W, Nam C, Li HL, Szpunar JA. Effects of local stress on the stability of tetragonal phase in ZrO_2 film. J Alloys Compd 2007;437:280–4.